Journal of the European Ceramic Society 22 (2002) 1051–1059
www.elsevier.com/locate/jeurceramsoc

Fracture behavior of AlN ceramics with rare earth oxides

R. Terao, J. Tatami, T. Meguro, K. Komeya*

Graduate School of Environment and Information Sciences of Engineering, Yokohama National University, 79-5, Tokiwadai, Hodogayaku, Yokohama, Kanagawa, 240-8501, Japan

Received 3 April 2001; accepted 17 July 2001

Abstract

The effect of three types of additives, Sm_2O_3, La_2O_3 and Y_2O_3, on the thermal and mechanical properties of AlN ceramics was investigated. Thermal conductivities of AlN ceramics with Sm_2O_3 and Y_2O_3 addition were 176 and 173 Wm^{-1} K^{-1}, respectively. However, in the case of La_2O_3 addition the value was limited to 101 Wm^{-1} K^{-1}. The strengths of AlN ceramics with Sm_2O_3 and La_2O_3 addition were 455 and 407 MPa, respectively, which are higher than that with Y_2O_3 addition. Fracture toughnesses of those with Sm_2O_3 and La_2O_3 addition were also higher than that with Y_2O_3 addition. The fracture behavior on the fracture surfaces was found to be a mixed mode of transgranular fracture and intergranular fracture. The specimens with Sm_2O_3 and La_2O_3 addition had more transgranular fracture than that with Y_2O_3 addition. The strengthening mechanism of Sm_2O_3 and La_2O_3 addition was clarified by using a theory on the fracture toughness considering the crack propagation path. As a result, we concluded that the improvement of strength and fracture toughness of AlN ceramics with Sm_2O_3 and La_2O_3 addition were mainly achieved by strengthening the grain boundary.

Keywords: AlN; Grain boundaries; Mechanical properties; Thermal properties; Toughness

1. Introduction

Aluminum nitride (AlN) is expected to be highly suitable for such applications as substrates and packages for IC/LSI, structural parts for semiconductor processes and filler for high thermal conductive resin because of its high thermal conductivity, excellent electrical insulation and thermal expansion coefficient close to that of silicon (Si).[1–4] In previous studies,[5–7] Y_2O_3 and CaO have been found to be better sintering aids for achievement of high density and high thermal conductivity. Then, high thermal conductive AlN parts were developed and put into practical application, but the expansion of their application is restricted in a low strength for AlN ceramics.[6,8] Therefore, in order to expand the applications of AlN, it is first of all necessary to develop stronger AlN ceramics with high thermal conductivity. As a point of interest, Komeya et al. discovered in previous research that the density and the strength of AlN ceramics were strongly influenced by rare earth oxides added as sintering aids. Although Sm_2O_3 and La_2O_3 addition have been more effective in strengthening AlN than the other rare earth oxides addition in the references, there are few reports on the sintering behavior and strengthening effect of these sintering aids. It has also been reported that AlN ceramics with various types of rare earth oxides addition have high thermal conductivity and have almost similar values of about 170 Wm^{-1} K^{-1}.[9] However, the strengthening mechanism of high thermal conductive AlN ceramics with Sm_2O_3 and La_2O_3 addition have not been made clear. Thus, the authors investigated the thermal and mechanical properties of AlN ceramics with Sm_2O_3, La_2O_3 and Y_2O_3 addition and clarified the strengthening mechanism as well as the phase reaction and sintering behavior.

2. Experimental

High purity and fine powders of AlN (Tokuyama Co., Ltd., F grade, 0.6 μm), La_2O_3 (Shinetsu Chemical Industry Co., Ltd., 0.7 μm) and Sm_2O_3 (Shinetsu Chemical Industry Co., Ltd., 0.4 μm) were prepared as raw materials. Y_2O_3 (Shinetsu Chemical Industry Co., Ltd., 0.6 μm) was used for a reference sintering aid. Table 1 shows the characteristics of the raw powders. It is noted

* Corresponding author. Fax: +81-45-339-3957.
E-mail address: komeya@ynu.ac.jp (K. Komeya).

PII: S0955-2219(01)00422-8

Table 1
Characteristics of raw powders

	AlN (Tokuyama Co.)		Y_2O_3 (Shinetsu Chem. Ind. Co.)		La_2O_3 (Shinetsu Chem. Ind. Co.)		Sm_2O_3 (Shinetsu Chem. Ind. Co.)	
Particle size (μm)	0.6		0.6		0.7		0.4	
BET ($m^2 g^{-1}$)	3.36		11.9		1.0		1.3	
Purity (mass%)	99.9		99.9		99.9		99.9	
Impurity (ppm)	O	8300	Dy_2O_3	<100	CeO_2	<50	Nd_2O_3	<100
	C	280	Ho_2O_3	<100	CaO	<50	Eu_2O_3	<100
	Si	280	Er_2O_3	<100	Pr_6O_{11}	<50	Gd_2O_3	<100
	Fe	<10	Yb_2O_3	<100	Nd_2O_3	<30	Pr_6O_{11}	<50
	Ca	7	CaO	<10	SiO_2	<30	CaO	<30

that the oxygen content in AlN powder is 0.8 wt.%. Batch compositions with 5 wt.% additives were prepared. The powder mixture was ball-milled in ethanol with a plastic pot and Al_2O_3 balls, and the ethanol was eliminated by evaporation. Paraffin was added to the mixed powder, which was molded into a pellet of 15 mm diameter by 5 mm thickness and a plate of 40 by 40 by 4 mm^3 under a uniaxial pressure of 50 MPa, followed by CIP at 200 MPa. Dewaxing was performed at 500 °C in air. The relative density of each green body was about 55%. The green bodies were fired at 1850 °C in N_2 for 2 h under 0.6 MPa. The relative density of the AlN sintered body was measured by the Archimede's method. Phases present and lattice constant of AlN were analyzed by X-ray diffraction with CuK_α radiation using Si powder as an internal standard. Sintered bodies were machined to the shape of 10 mm diameter by 2 mm thickness to measure thermal conductivity by the CO_2 laser flash method[10] and to that of 3×3×30 mm^3 to measure bend strength and fracture toughness. The bend strength was measured by a 3-point bending test with a span of 16 mm and a crosshead speed of 0.5 mm/min, and fracture toughness was measured by the surface crack in flexure (SCF) method.[11] Microstructure was observed by a scanning electron microscope (SEM) and a transmission electron microscope (TEM). Fractured surface was evaluated by SEM using the specimen after fracture toughness tests.

3. Results and discussion

3.1. Sinterability

Table 2 summarizes the characteristics of sintered AlN specimens. Full densification was achieved through the liquid phase sintering process in each specimen. This phenomenon can be understood by the eutectic point in

Table 2
Properties of sintered AlN specimens

Composition	5 mass% Y_2O_3	5 mass% La_2O_3	5 mass% Sm_2O_3
Density ($g\ cm^{-3}$)	3.25	3.27	3.30
Phases present	AlN $Y_4Al_2O_9$	AlN $LaAlO_3$	AlN $SmAlO_3$
Mean grain size (μm)	4.0	4.0	3.3
Thermal conductivity ($Wm^{-1} K^{-1}$)	173	101	176
Thermal diffusivity ($cm^2 s^{-1}$)	(0.75)	(0.44)	(0.76)
Lattice constant c (Å)	4.9794	4.9787	4.9796
Standard deviation (±Å)	(0.0002)	(0.0001)	(0.0002)
Bending strength σ_f (MPa)	353	407	455
Standard deviation (±MPa)	(30)	(40)	(54)
Fracture toughness K_{IC} (MPa $m^{1/2}$)	2.9	3.0	3.1
Standard deviation (±MPa $m^{1/2}$)	(0.1)	(0.1)	(0.1)
Fraction of transgranular fracture $\hat{f}$ (%)	23	57	40
Disappeared fracture energy ($J\ m^{-2}$)	28	30	32
Standard deviation (±$J\ m^{-2}$)	(2)	(2)	(2)
Fracture toughness of grain G_{IC}^{grain} ($J\ m^{-2}$)	43	36	43
Fracture toughness of grain boundary $G_{IC}^{boundary}$ ($J\ m^{-2}$)	8	11	10

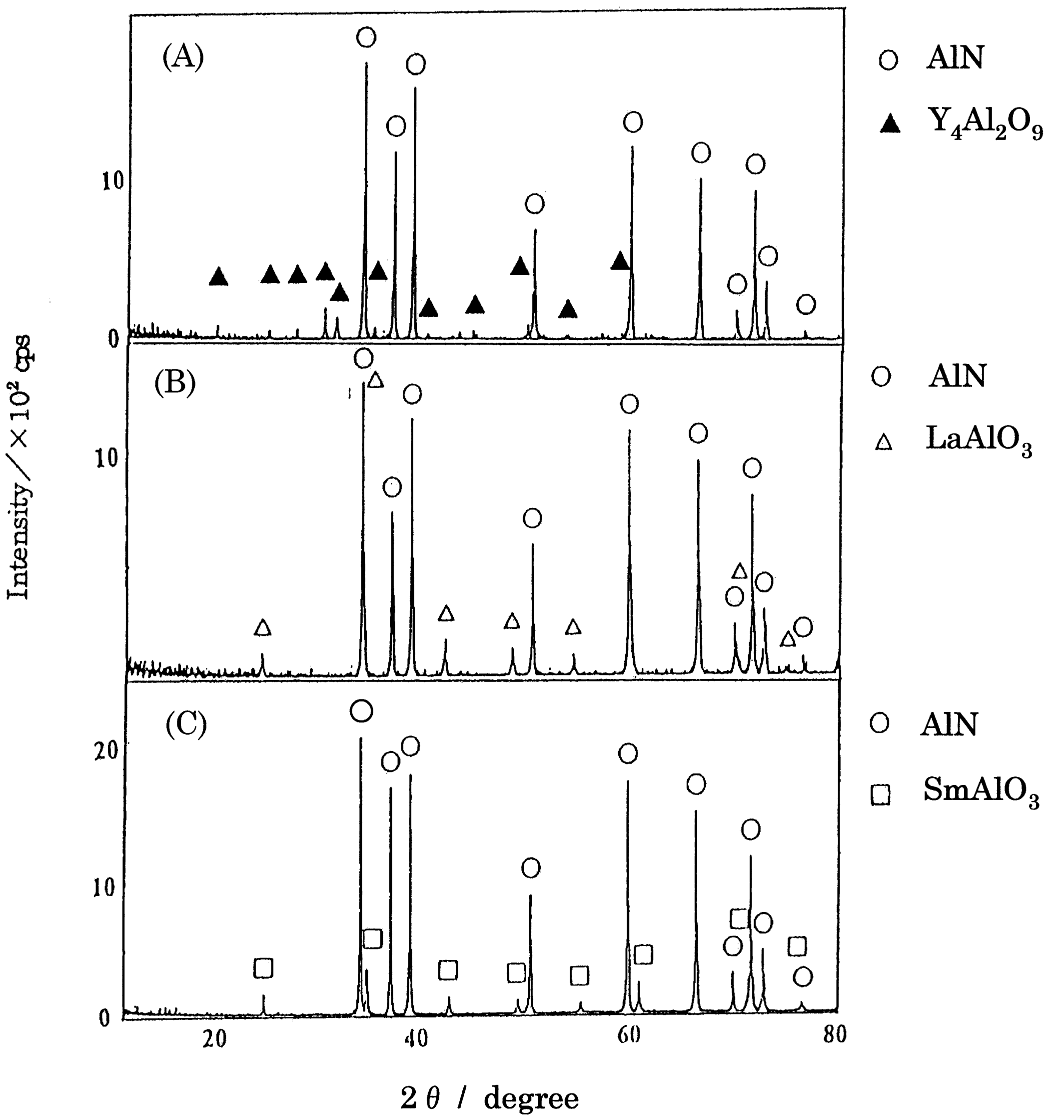

Fig. 1. X-ray diffraction profiles of AlN with (A) 5 mass% Y_2O_3, (B) 5 mass% La_2O_3 and (C) 5 mass% Sm_2O_3.

the binary system of Al_2O_3 and additives, namely 1760 °C for the Y_2O_3 addition,[12] 1830 °C for La_2O_3 addition[13] and 1825 °C for Sm_2O_3 addition.[14] Fig. 1 illustrates XRD profiles of the sintered specimens. AlN was identified as a main phase. However, second phases of AlN ceramics with Sm_2O_3 and La_2O_3 addition were identified as Perovskite types formed by the reaction with Al_2O_3, whereas that with Y_2O_3 addition is identified as monoclinic type.[15]

3.2. Thermal conductivity

Thermal conductivity shown in Table 2 is scattered in the range of 101–176 $Wm^{-1}\ K^{-1}$ in the three specimens: 173 $Wm^{-1}\ K^{-1}$ for Y_2O_3 addition, 101 $Wm^{-1}\ K^{-1}$ for La_2O_3 addition and 176 $Wm^{-1}\ K^{-1}$ for Sm_2O_3 addition. This difference is considered to be related to their microstructures. Fig. 2 shows SEM photographs of fracture surfaces of sintered AlN specimens. The microstructures were composed of isotropic AlN grains and grain boundary phases for all specimens. The grain size estimated was 3.3 μm for Sm_2O_3 addition, 4.0 μm for La_2O_3 addition and 4.0 μm for Y_2O_3 addition by the intercept method, in which the number of measured grains was about 200. Fig. 3 shows typical TEM photographs of sintered AlN specimens. The dihedral angle of La_2O_3 addition is smaller than those of other additions, meaning that wettability is better. Fig. 4 shows lattice constant c and the thermal conductivity of sintered AlN specimens. In this figure, lattice constant *c* of AlN with La_2O_3 is shorter than those with Y_2O_3 and Sm_2O_3 additions. Therefore, The AlN grain in the specimen with La_2O_3 addition is considered to contain more oxygen than that with Y_2O_3 and Sm_2O_3 addition. Since the oxygen in the AlN grain and the grain boundary disturbs phonon transfer,[16–19] the thermal conductivity of

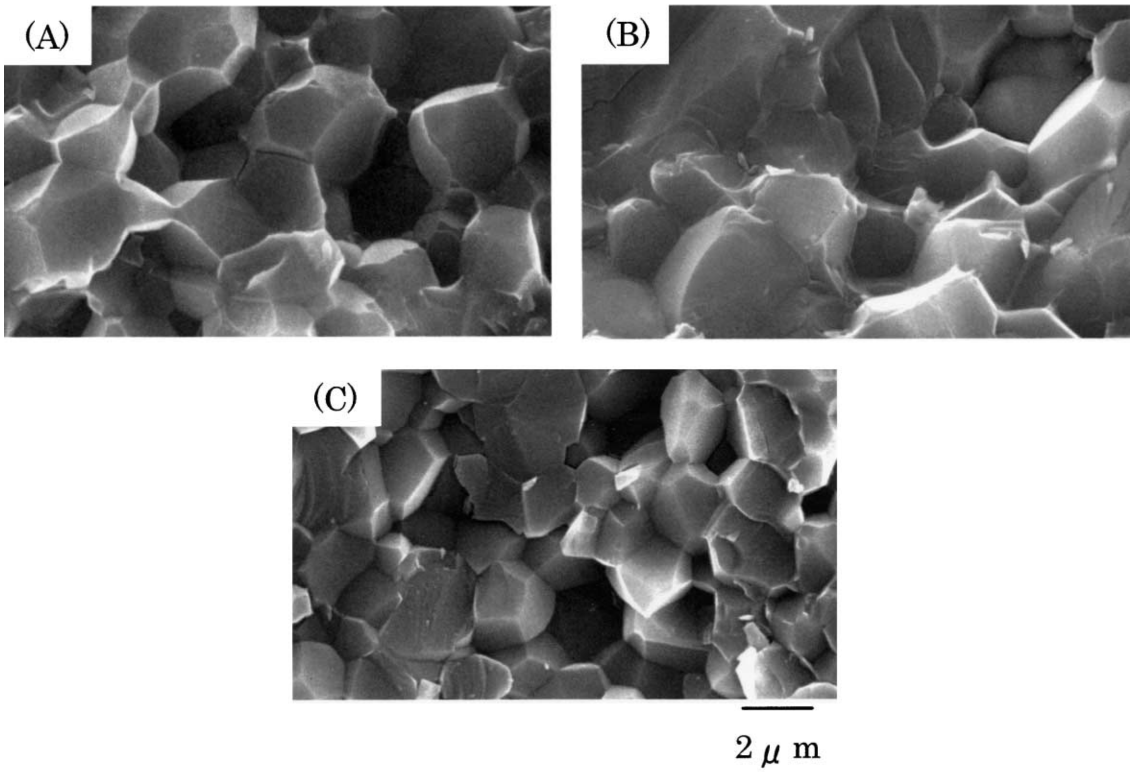

Fig. 2. SEM photographs of fractured surface of AlN with (A) 5 mass% Y_2O_3, (B) 5 mass% La_2O_3 and (C) 5 mass% Sm_2O_3. Those pictures were taken at around 100 μm below fracture origin perpendicularly. Average grain size of AlN is (A) 4.0, (B) 4.0 and (C) 3.3 μm, respectively.

AlN ceramics with La_2O_3 addition seems lower than those with Sm_2O_3 and Y_2O_3 addition. A delayed reaction between Al_2O_3 in AlN and La_2O_3 addition would influence microstructure and thermal conductivity, because the particles of raw La_2O_3 powder are coarser than those of raw Sm_2O_3 and Y_2O_3 powders.

3.3. Strength and fracture toughness

Fig. 5 illustrates the bend strength and the fracture toughness of AlN ceramics with Sm_2O_3, La_2O_3 and Y_2O_3 addition. The bending strengths of AlN ceramics with Sm_2O_3 and La_2O_3 addition were 455 and 407 MPa, respectively, which are about 50–100 MPa higher than that with Y_2O_3 addition. Furthermore, the fracture toughnesses with Sm_2O_3 and La_2O_3 addition were 3.1 and 3.0 MPa $m^{1/2}$, respectively, whereas that with Y_2O_3 addition was 2.9 MPa $m^{1/2}$. It is significant to recognize that both bend strength and fracture toughness were simultaneously increased by Sm_2O_3 and La_2O_3 addition. Although the difference of these fracture toughnesses is small, their standard deviations have also a quite small value ($= \pm 0.1$ MPam$^{1/2} =$ 3% of K_{IC}) and we obtained similar results on the relationship between fracture toughnesses and fracture behavior of AlN ceramics with Y_2O_3,[20] we regarded them as different value to carry out following discussion.

According to linear fracture mechanics, the strength (σ_f) is expressed by Eq. (1).[21]

$$\sigma_f = \frac{K_{IC}}{Y\sqrt{C}} \tag{1}$$

where K_{IC} is fracture toughness, C is flaw size and Y is a geometrical constant. This equation explains that strength is proportional to fracture toughness and $C^{-1/2}$. The strength of La_2O_3 addition is higher than that of Y_2O_3 addition, although grain size of La_2O_3 addition is the same as that of Y_2O_3 addition. It is considered that strengthening of La_2O_3 addition is achieved by an improvement of fracture toughness, because fracture toughness of La_2O_3 addition is higher than that of Y_2O_3 addition. On the other hand, grain size of Sm_2O_3 is smaller than that of Y_2O_3 addition. Judging from the result of La_2O_3 addition, it seems that strengthening of Sm_2O_3 addition is influenced by not only grain size but also the improvement of fracture toughness.

3.4. Fracture behavior

In order to investigate toughening mechanism of Sm_2O_3 and La_2O_3 addition, their fracture behavior of SCF specimen were estimated. As shown in Fig. 2, fracture surfaces of Sm_2O_3 and La_2O_3 addition exhib-

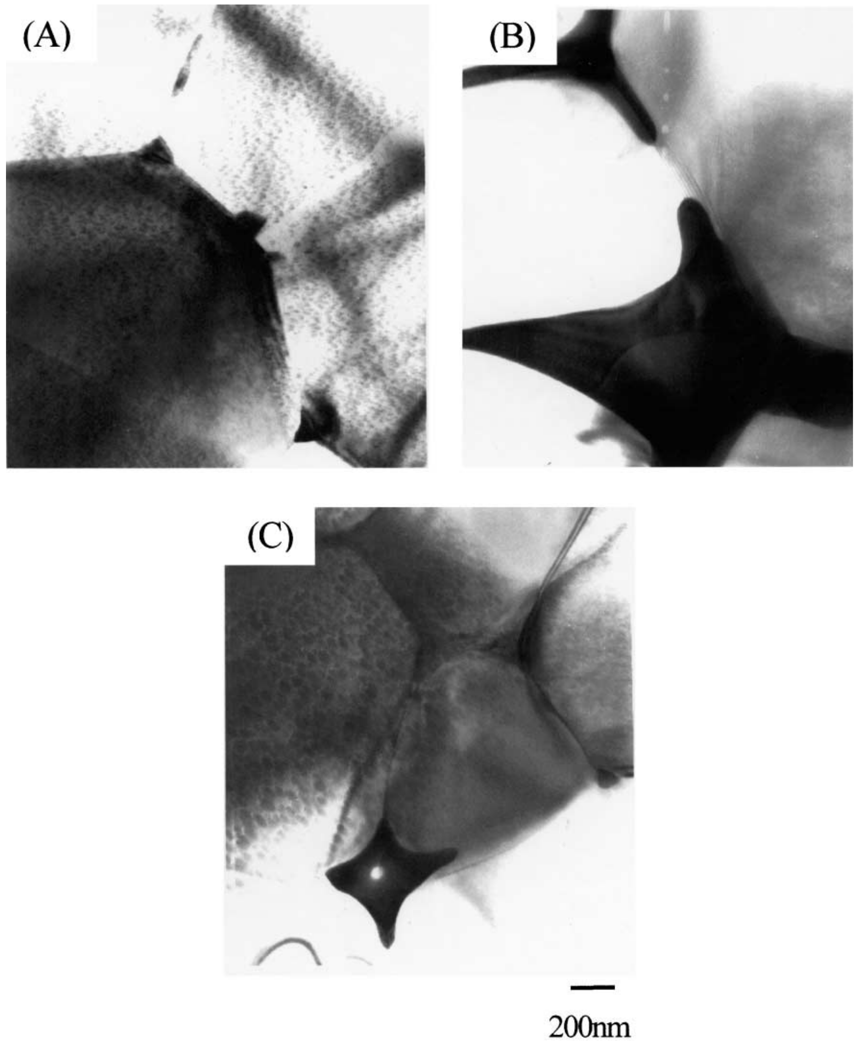

Fig. 3. TEM photographs of AlN with (A) 5 mass% Y_2O_3, (B) 5 mass% La_2O_3 and (C) 5 mass% Sm_2O_3. Conditions of dihedral angle and grain boundary: (A) width and thinness, (B) narrow and thickness and (C) width and thinness, respectively.

ited transgranular fractures as well as intergranular fracture, although fracture surface of Y_2O_3 addition exhibited almost intergranular fracture. The fraction of transgranular fractures was calculated by the number of the transgranular fractured grains over the number of the grains observed in several SEM photographs.[22] Approximately 200 grains were measured for the calculation. The fraction of transgranular fracture was 40% in Sm_2O_3 addition and 57% in La_2O_3 addition, whereas that of Y_2O_3 addition was 23%. Sm_2O_3 and La_2O_3 addition with high fracture toughness and high strength had more transgranular fracture than a Y_2O_3 addition. In order to find out the toughening mechanism of Sm_2O_3 and La_2O_3 addition, the theory[23] of the influence of the crack path on the fracture toughness of polycrystalline ceramics with a stochastic model based on the difference between the released energies in intergranular and transgranular crack propagation was used. In this theory, the expected values of the fraction of transgranular fracture on fracture surface, $\hat{f}$, and the critical energy release rate, $\hat{G}_{IC}$, of polycrystalline ceramics were formulated as functions of grain size d, the fracture toughness of grain, G_{IC}^{grain}, and grain boundary, $G_{Ic}^{boundary}$, were formulated as follows,

$$\hat{f} = \frac{\mathrm{d} - 2y_c}{d} \tag{2}$$

$$\hat{G}_{IC} = G_{IC}^{grain}\left(1 - \frac{2y_C}{\mathrm{d}}\right) + G_{IC}^{boundary}\left\{1 + \frac{p}{6d}y_C^2 + \frac{q}{2d}y_C\right\}\frac{2y_C}{\mathrm{d}} \tag{3}$$

where,

$$p = \frac{p'}{2a} \tag{4}$$

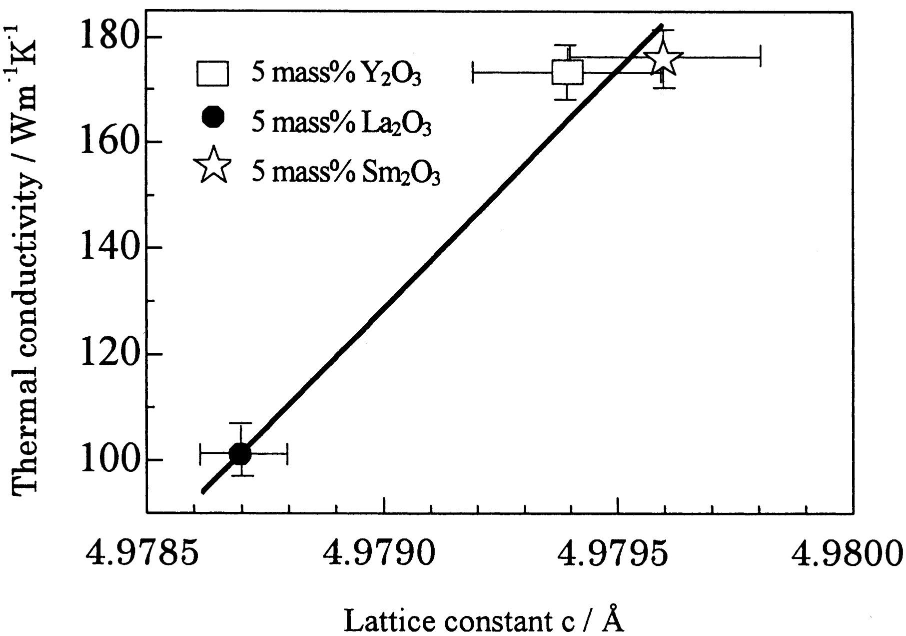

Fig. 4. Lattice constant *c* versus thermal conductivity of sintered AlN with 5 mass% Y_2O_3, 5 mass% La_2O_3 and 5 mass% Sm_2O_3.

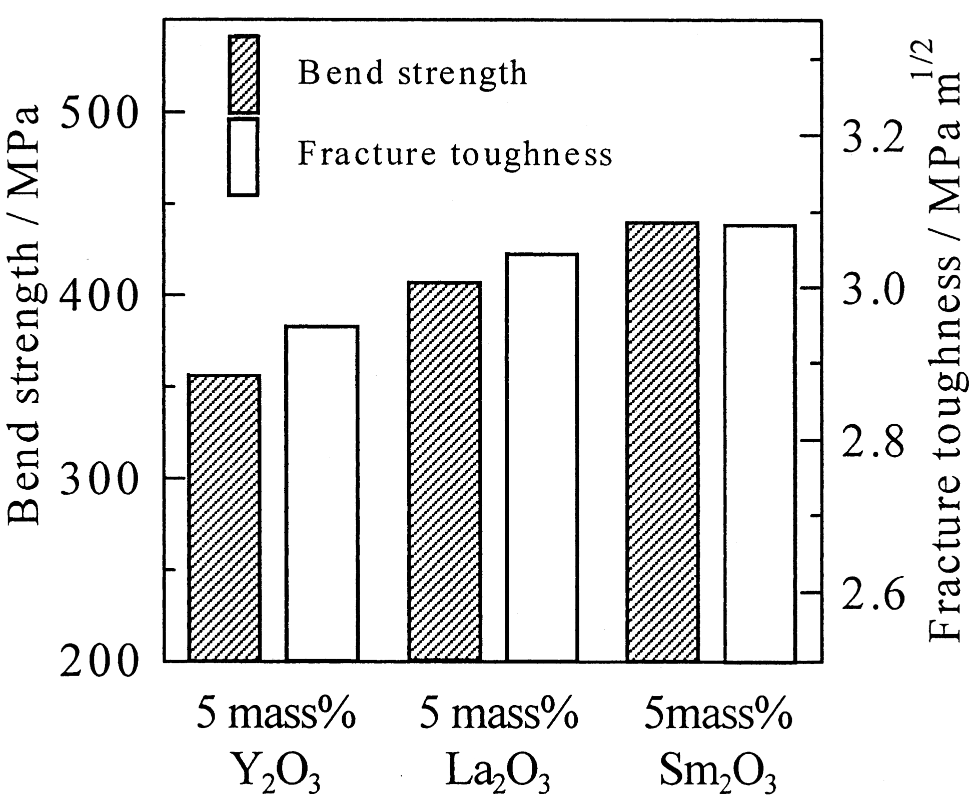

Fig. 5. Bend strength and fracture toughness of sintered AlN with 5 mass% Y_2O_3, 5 mass% La_2O_3 and 5 mass% Sm_2O_3.

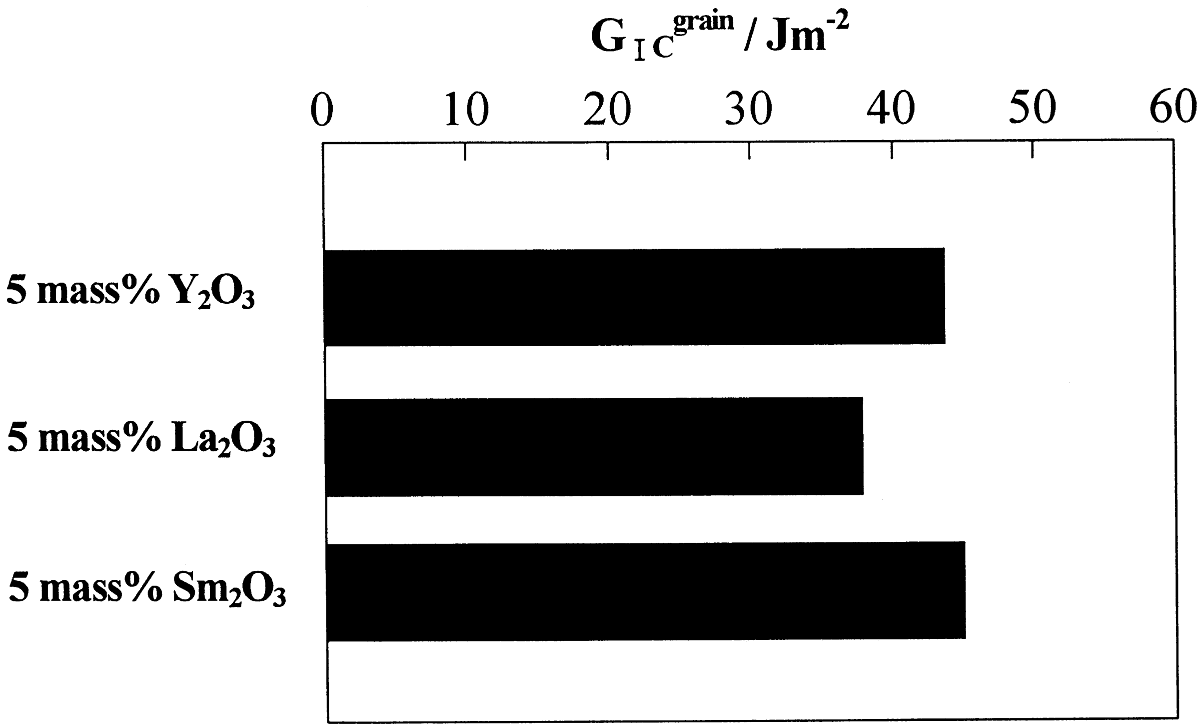

Fig. 6. Fracture toughness of grain in sintered AlN specimens.

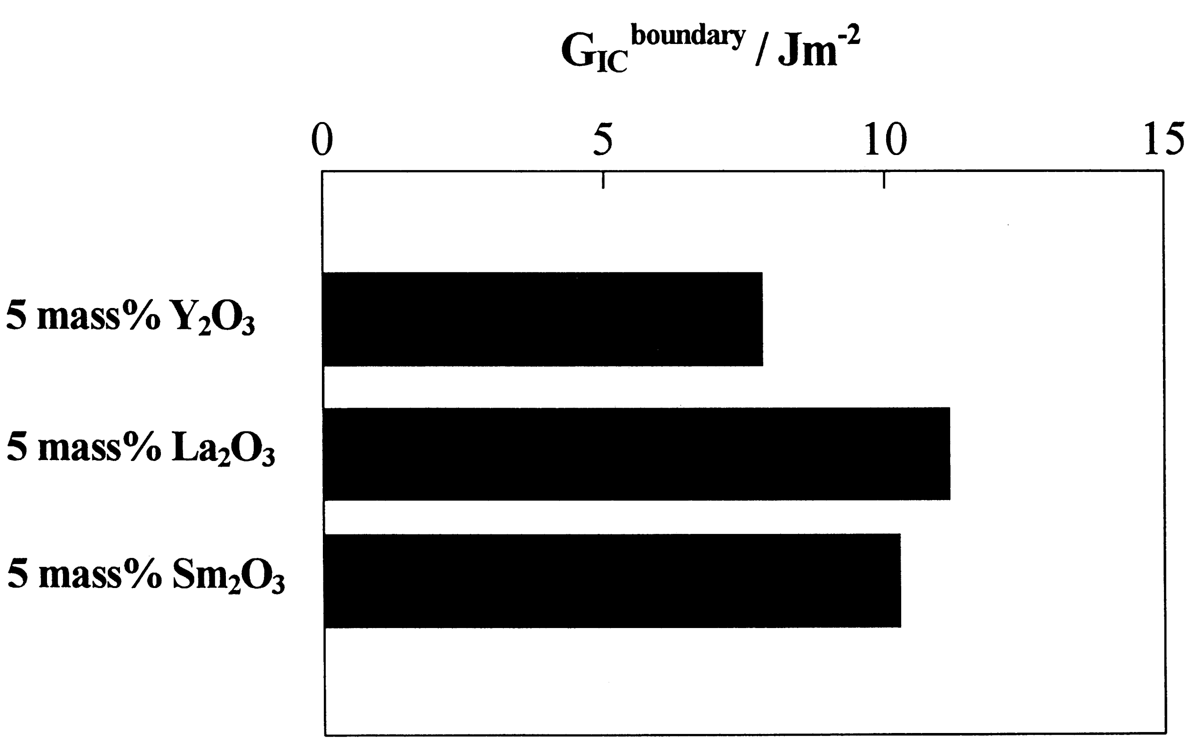

Fig. 7. Fracture toughness of grain boundary in sintered AlN specimens.

$$y_C = \begin{cases} \dfrac{-q + \sqrt{q^2 + 2\left(\dfrac{G_{IC}^{grain}}{G_{IC}^{boundary}} - 1\right)pd}}{p} & (d \geqslant d^*) \\ \dfrac{d}{2} & (0 < d < d^*) \end{cases} \quad (5)$$

$$d^* = \frac{8\left(\dfrac{G_{IC}^{grain}}{G_{IC}^{boundary}} - 1\right) - 4q}{p} \quad (6)$$

p', q: constants

These equations were drived from an assumption that when a crack propagates in the selective region of intergranular fracture with a length y_C, the crack propagates intergranularly. It should be noted that the intergranular fracture includes not only the fracture of the interface between AlN grains and the secondary phase. d* is calculated from the condition of $y_C \leqslant d/2$, which is the critical grain size for transgranular fracture. This theory was verified in polycrystalline alumina with equiaxed grains. AlN ceramics in this paper has also equiaxed grains, so the above theory seems to be satisfactory. By substituting the experimental data of the grain size, d, the fraction of transgranular fracture f and the critical energy release rate G_{IC} for Eqs. (2)–(6). The fracture toughnesses of grain, G_{IC}^{grain}, and grain boundary, $G_{IC}^{boundary}$, were calculated. G_{IC} was converted from Irwin's equation[24] in this study by setting 280 GPa for Young's modulus and 0.25 for Poisson ratio. The crack length a was set to 100 μm, which is almost equal to the crack length of the SCF method.

Fig. 6 shows calculated value of the fracture toughness of AlN grain. The fracture toughnesses of AlN grain in the specimen with Sm_2O_3 and Y_2O_3 addition were 43 and 43 J m^{-2}, respectively. While, that of the La_2O_3 addition was 36 J m^{-2}, namely, the AlN grain in specimen with the Sm_2O_3 and Y_2O_3 addition was strengthened. It is considered that oxygen in AlN grain makes AlN grain weak, because the desoluted oxygen form vacancy at AlN site and stacking fault.[25] The reason why AlN grain was weaken by La_2O_3 addition is that AlN grain in the specimen with La_2O_3 addition had more oxygen content than that with Sm_2O_3 and Y_2O_3 addition as mention above. This result also means that the improvement of the fracture toughness of AlN grain and the thermal conductivity simultaneously achieves.

Fig. 7 shows the fracture toughness of the grain boundary of AlN specimens. The fracture toughness of the grain boundary for Sm_2O_3 and La_2O_3 addition is 10 and 11 J m^{-2}, respectively, while that with the Y_2O_3 addition is 8 J m^{-2}. In this work, the grain boundary of AlN for Y_2O_3 addition was $Y_4Al_2O_9$, whereas the grain boundary of AlN for Sm_2O_3 and La_2O_3 addition was Perovskite type compound. Although we consider that the fracture toughness of the grain boundary depends on the grain boundary phase, they have not been clarified at this time. In the future work, we hope that strengthening mechanism of the grain boundary will be made clear by direct measurement of fracture toughness of their grain boundary with AlN bycristals and/or analysis of grain boundary structure with TEM.

4. Conclusion

Fracture behavior of AlN ceramics with rare earth oxides was investigated. Both Sm_2O_3 and La_2O_3 promoted the densification of AlN as well as Y_2O_3 addition, which is based on the liquid phase formed in the Al_2O_3-rare earth oxide systems. Thermal conductivities of the sintered bodies with Sm_2O_3 and Y_2O_3 are 176 and 173 W m^{-1}K^{-1}, respectively, whereas the value was limited to 101 W m^{-1}K^{-1} for La_2O_3 addition because of lower dihedral angle between solid-liquid phases and higher oxygen content in AlN grain of the specimen with La_2O_3 addition. Strengths of 455 and 407 MPa were obtained using Sm_2O_3 and La_2O_3 addition, respectively. These values are higher than that for Y_2O_3 addition. Many transgranular fractured grains were observed in the fractured surfaces of the two high strength specimens. By substitution of the experimental data into the theory of fracture toughness and fracture behavior of polycrystalline ceramics, the fracture toughness of AlN grain and grain boundary was estimated. The fracture toughness of AlN grain increased with an increase in the length of c-axis of AlN, namely, with a decrease of oxygen content in AlN grain. This means that the fracture toughness of AlN grain and thermal conductivity simultaneously improve. The fracture toughness of grain boundary from Sm_2O_3 and La_2O_3 addition was higher than that from the Y_2O_3 addition. It should be possible to strengthen the grain boundary phase and/or phase boundary between AlN grain and grain boundary phase by using Sm_2O_3 and La_2O_3 addition.

References

1. Baik, Y. and Drew, R. A. L., Aluminum nitride: processing and applications. *Key Engineering Materials*, 1996, **122–124**, 553–570.
2. Blakely, K. A., Martin, S. C. and Spohn, M. T., Material supplier's role in market development. *Am. Ceram. Soc. Bull.*, 1995, **74**, 55–58.
3. Sheppard, L. M., Aluminum nitride. *Am. Ceram. Bull.*, 1990, **69**, 1801–1812.
4. Kuramoto, N., Taniguchi, H. and Aso, I. Development of highly thermal conductive AlN substrate by green sheet technology. Proceedings of the 36th Electronic Components Conference. IEEE Compon. Hybrids Manuf. Tech. Soc., Piscataway, NJ, 1986, pp. 424–429.

5. Komeya, K. and Inoue, H., The Influence of Fibrous Aluminum Nitride on the Strength of Sintered AlN–Y_2O_3. *Trans. J. Brit. Ceram Soc*., 1971, **70**, 107–113.
6. Komeya, K., Inoue, H. and Tsuge, A., Effect of various additives on sintering of aluminum nitride. *Yogyo Kyokaishi*, 1981, **89**, 330–336.
7. Schuster, J. C., Phase diagrams relevant for sintering aluminum nitride based ceramics. *Rev. Chim. Miner*., 1987, **24**, 676–686.
8. Witek, S. R., Miller, G. A. and Harmer, M. P., Effects of CaO on strength and toughness of AlN. *J. Am. Ceram. Soc*., 1989, **72**, 469–473.
9. Jackson, T. B., Virkar, A. V., More, K. L., Dinwiddie Jr., R. B. and Cutler, R. A., High-thermal-conductivity aluminum nitride ceramics. *J. Am. Ceram. Soc*., 1997, **80**, 1421–1435.
10. Enck, R. C., Harris, R. D. and Youngman, R. A., Measurement of the thermal diffusivity of translucent aluminum nitride. *Ceramic Transactions*, 1989, **5**, 214–221.
11. ASTM C1421-99, Standard test methods for determination of fracture toughness of advanced ceramics at ambient temperature, pp. 1–32.
12. Toropov, N. A., *Izv. Akad. NauK SSSR, Ser. Khim*., 1964, **7**, 1162.
13. Bonder, I. A., *Izv. Akad. NauK SSSR, Ser. Khim*., 1964, **5**, 7885.
14. Bonder, I. A., *Izv. Akad. NauK SSSR, Ser. Khim*., 1966, **2**, 213.
15. Schneider, S. J., Roth, R. S. and Waring, J. L., Solid state reactions involving oxides of trivalent cation. *J. Research NBS*, 1961, **65A**(4), 345–347.
16. Slack, G. A., Nonmetallic crystals with high thermal conductivity. *J. Phys. Chem. Solids*, 1973, **34**, 321–335.
17. Buhr, H. and Müller, G., Microstructure and thermal conductivity of AlN(Y_2O_3) ceramics sintered in different atmospheres. *J. Eur. Ceram. Soc*., 1993, **12**, 271–277.
18. Streicher, E., Chartier, T., Boch, P., Denanot, M.-F., Rabier, J., Densification and thermal conductivity of low-sintering-temparature AlN materials. *J. Eur. Ceram. Soc*., 1990, **6**, 23–29.
19. Okamoto, M., Arakawa, H., Oohashi, M. and Ogihara, S., Effect of microstructure on thermal conductivity of AlN ceramics. *J. Ceram. Soc. Japan*, 1989, **93**, 1478–1485.
20. Tatami, J., Komeya, K., Meguro, T., Iwasawa, S. and Terao, R., Fracture behavior of strengthened AlN. *Ceramic Transaction*, 2000, **106**, 493–499.
21. Irwin, G. R. and Kies, J. A., Fracturing and fracture dynamics. *Weld. J. Res. Sup*, 1952, **31**(2), 95s–100s.
22. Yasuda, K., Tatami, J., Matsuo, Y. and Kimura, S., Influence of crack propagation path on the fracture toughness of polycrystalline Al_2O_3. *J. Ceram. Soc. Japan*, 1994, **102**, 887–889.
23. Tatami, J., Yasuda, K., Matsuo, Y. and Kimura, S., Stochastic analysis on crack path of polycrystalline ceramics based on the difference between the released energies in crack propagation. *J. Mater. Sci*., 1997, **32**, 2341–2346.
24. Irwin, G. R., Analysis of stresses and strains near the end of a crack traversing a plate. *J. Appl. Mech.Trans*, 1957, **24**, 361–364.
25. Watari, K., Brito, M. E., Yasuoka, M., Valecillos, M. C., Kanzaki, S., Influence of powder characteristics on sintering process and thermal conductivity of aluminum nitride ceramics. *J. Ceram. Soc. Jpn*., 1995, **103**(9), 891–900.